Fundamental Research 5 (2025) 103–114

Contents lists available at ScienceDirect

Fundamental Research

journal homepage: http://www.keaipublishing.com/en/journals/fundamental-research/

Article

Critical biomarkers for responsive deep brain stimulation and responsive focal cortex stimulation in epilepsy field

Zhikai Yu[a,d,1], Binghao Yang[b,e,1], Penghu Wei[a,c], Hang Xu[a,d], Yongzhi Shan[a,c], Xiaotong Fan[a,c], Huaqiang Zhang[a,c], Changming Wang[a,d], Jingjing Wang[a,c,d,*], Shan Yu[b,e,*], Guoguang Zhao[a,c,d,*]

[a] Department of Neurosurgery, Xuanwu Hospital, Capital Medical University, Beijing 100053, China
[b] Laboratory of Brain Atlas and Brain Inspired Intelligence, Institute of Automation, Chinese Academy of Science, Beijing 100190, China
[c] Clinical Research Center for Epilepsy, Capital Medical University, Beijing 100053, China
[d] Laboratory of Brain Inspired Intelligence, Capital Medical University, Beijing 100053, China
[e] School of Future Technology, University of Chinese Academy of Science, Beijing 101408, China

ARTICLE INFO

Article history:
Received 27 December 2023
Received in revised form 11 May 2024
Accepted 30 May 2024
Available online 24 June 2024

Keywords:
Biomarker
Critical state
Feedback electrical stimulation
Epilepsy
Brain computer interface

ABSTRACT

To derive critical signal features from intracranial electroencephalograms of epileptic patients in order to design instructions for feedback-type electrical stimulation systems. The Detrended Fluctuation Analysis (DFA) exponent is chosen as the classification exponent, and the disparities between indicators representing distinct seizure states and the classification efficacy of rudimentary machine learning models are computed. The DFA exponent exhibited a statistically significant variation among the pre-ictal, ictal period, and post-ictal stages. The Linear Discriminant Analysis model demonstrates the highest accuracy among the three basic machine learning models, whereas the Naive Bayesian model necessitates the least amount of computational and storage space. The set of DFA exponents is employed as an intermediary variable in the machine learning process. The resultant model possesses the capability to function as a feedback trigger program for electrical stimulation systems of the feedback variety, specifically within the domain of neural modulation in epilepsy.

1. Introduction

An emerging treatment method for mental and neurological disorders, intracranial electrical stimulation, provides substantial therapeutic effects for incurable diseases without impairing brain function [1,2]. The intracranial electrical stimulation system, a significant domain within neural modulation technology, has demonstrated remarkable progress in the treatment of motor disorders such as Parkinson's disease [3,4], as well as dependable evidence in the realm of depression treatment [5,6]. Indeed, surgeons can address these diseases that share neural pathways by inserting the stimulation electrodes of the transcranial electrical stimulation system into a common target, such as the subthalamic nucleus (as is most frequently observed in the treatment of Parkinson's disease) [7]. Post-operatively, patients can benefit from fixed frequency stimulation with an electrical stimulator, such as 100 Hz electrical stimulation, which aids in the elimination or reduction of the disease's detrimental effects [8]. Nevertheless, in the case of epilepsy, a condition characterized by intricately unique neural pathways, the utilization of stimulation electrodes on a standardized target for induction fails to yield optimal outcomes [9]. In light of this, the stimulation target was modified to correspond with the epileptic lesion. Further investigation revealed that while electrical stimulation of the lesion did not appear to have a significant impact during the interictal phase, it could effectively interrupt this episode before or during its onset. Consequently, in pursuit of energy conservation and to preserve the functionality of brain regions associated with non-seizure lesion sites unaffected by electrical stimulation, Neuro Pace researchers integrated the notion of closed-loop control into the blueprint for intracranial electrical stimulators. This resulted in the development of the Responsive Neuro Stimulation (RNS) system, the pioneering feedback type of electrical stimulation system [10].

While intricate circuit structures may be present in feedback electrical stimulation systems (Fig. 1A), they can be succinctly described as comprising three components: recording electrodes, stimulating electrodes, and feedback triggers (Fig. 1B). The stimulating electrode will discharge in response to aberrant signal characteristics detected by the

* Corresponding authors.
E-mail addresses: wang-jj94@xwhosp.org (J. Wang), shan.yu@nlpr.ia.ac.cn (S. Yu), ggzhao@vip.sina.com (G. Zhao).
[1] These authors contributed equally to this work.

https://doi.org/10.1016/j.fmre.2024.05.018

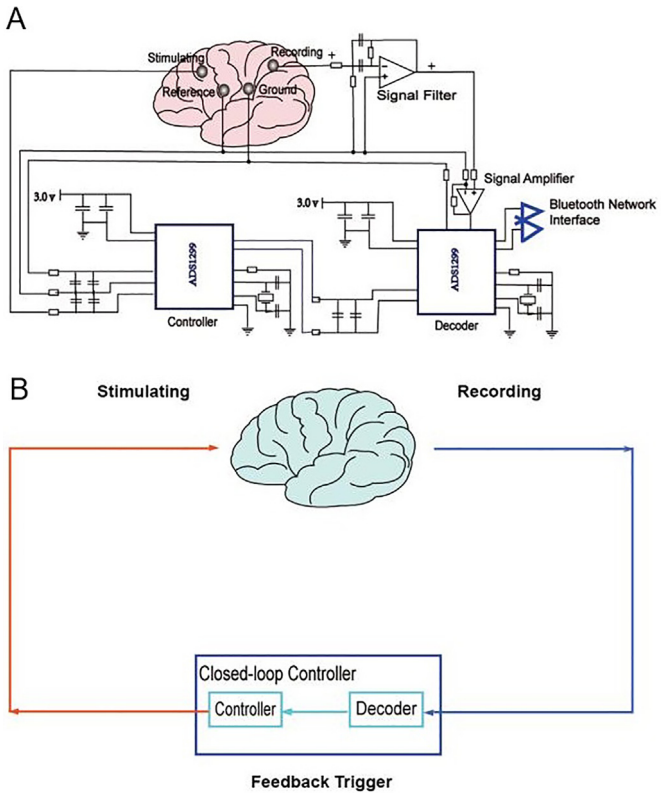

Fig. 1. Electronic design for feedback type of epilepsy stimulator. (A) Detailed wiring diagram. (B) Simplified block diagram.

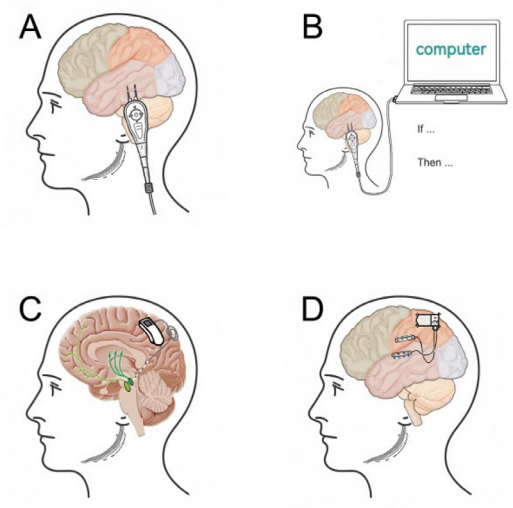

Fig. 2. Feedback stimulators in anatomical localization. (A) A very simplified electrical stimulator with open loop. (B) A very simplified electrical stimulator with closed loop. (C) DBS with closed loop and integrated to an all-in-one machine. (D) FCS with closed loop and integrated to an all-in-one machine.

recording electrode via the feedback trigger. Initially, enterprise engineers implemented the RNS system by concurrently utilizing three indicators—line length, area, and half wave—to ascertain the presence of epilepsy seizures, which served as prerequisites for feedback triggers that stimulated electrode discharge. While the concurrent utilization of these three indicators yields a detection accuracy approaching 100% [9], the implementation of intricate algorithms necessitates substantial computational power, leading to escalated energy consumption and hardware performance demands [11]. This is particularly detrimental for implantable systems that have restricted battery capacity. In light of advancements in machine learning techniques, scholars from various research groups have put forth feedback-triggered algorithms that leverage machine learning principles to mitigate the need for substantial computational resources [11–14]. On the contrary, artificial intelligence approaches that rely on unprocessed data as a training set necessitate the ingestion of an enormous training dataset into the implanted system. This not only necessitates a substantial amount of storage but is also detrimental to implanted systems that have restricted circuit capacity. Therefore, is there an indicator derived from traditional analytical modeling techniques that can function as an intermediary variable in machine learning algorithms to determine the period of a seizure, optimizing storage and computing power and reducing algorithm complexity while maintaining algorithm accuracy?

The critical state theory represents a significant trajectory within the domain of complex science [15]. The observation that the intracranial electrical signals of individuals with epilepsy progress through three discrete critical states—pre-ictal, ictal, and post-ictal—is quite intriguing. The Detrended Fluctuation Analysis (DFA) Exponent represents the characteristic of long-range temporal correlation (LRTC) [16–18], which measures scaling behavior emerging from the balanced excitation/inhibition (E/I) network, and reflects the capability of information process in the neuronal network. Therefore, DFA exponent can be used to analyze the change of the brain state or disorders corresponding to the variation of network E/I. In detail, previous studies indicated the decline of DFA exponent during sleep deprivation [18]. Furthermore, multiple neurological disorders, such as Alzheimer's diseases [19] or autism [20], are related with the variation of DFA exponent. So it was chosen as an indicator to differentiate between states preceding and following epileptic convulsions, in accordance with the critical state theory. The classification accuracy of this indicator was verified using the publicly available OpenNeuro dataset [21]. While the primary objective of this article is to decrease computational and storage demands, it is still imperative to validate the DFA exponent's classification accuracy. This is because attaining results that simultaneously minimize the computational and storage demands of the system and uphold a high level of classification accuracy is the only thing that holds significance. Additionally, considering the categorization of stereo electroencephalograms (SEEG) and electrocorticography (ECoG) among patients with epilepsy, we conducted a comparative analysis of the DFA exponents' performance across both data types. The two data categories correspond to the data sources utilized for responsive Deep Brain Stimulation (rDBS) and responsive Focal Cortical Stimulation (rFCS), in practical terms. As a result, responsive Deep Brain Stimulation [22] and responsive Focal Cortical Stimulation [23], which correspond to open-loop Deep Brain Stimulation and open-loop Focal Cortical Stimulation, are distinguished in this article (Fig. 2C-D), to avoid designating them consistently as Responsive Neuro Stimulation (RNS) (Fig. 2A-B).

The innovation of this article resides in: (1) Dividing responsive Deep Brain Stimulation from responsive Focal Cortical Stimulation instead of naming them RNS together, and proving that there are substantial distinctions in signal properties between the two data types, such as SEEG and ECoG. (2) The effectiveness of employing DFA exponent as a feedback trigger indicator has been established, as it demonstrates commendable signal classification capabilities across various epilepsy stages. This research presents a pragmatic scenario in which critical state theory is implemented. (3) We incorporate an intermediary variable utilized in machine learning algorithms for feedback-based electrical stimulation. By performing intermediate variable calculations prior to training machine learning models, substantial computational and storage demands are significantly mitigated.

Table 1
Clinical information of patients without private identifiers.

participant_id	age	sex	hand	outcome	engel	therapy	implant	target	lesion_status	age_onset
sub-HUP060	42	F	R	F	3A	ABLATION	SEEG	FRONTAL	n/a	12
sub-HUP064	21	M	L	S	1D	RESECTION	ECOG	FRONTAL	LESIONAL	3
sub-HUP065	36	M	R	S	1B	RESECTION	ECOG	TEMPORAL	LESIONAL	2
sub-HUP074	25	F	L	S	1C	RESECTION	ECOG	TEMPORAL	LESIONAL	5
sub-HUP075	57	F	L	F	4A	RESECTION	ECOG	TEMPORAL	NON-LESIONAL	52
sub-HUP080	n/a	F	L	F	2C	RESECTION	ECOG	TEMPORAL	NON-LESIONAL	n/a
sub-HUP086	25	F	L	S	2A	RESECTION	ECOG	TEMPORAL	NON-LESIONAL	17
sub-HUP088	35	F	L	S	1D	RESECTION	ECOG	TEMPORAL	LESIONAL	1
sub-HUP089	n/a	n/a	n/a	S	1B	RESECTION	ECOG	n/a	n/a	n/a
sub-HUP094	48	F	R	S	1B	RESECTION	ECOG	TEMPORAL	NON-LESIONAL	20
sub-HUP105	39	M	R	S	1A	RESECTION	ECOG	TEMPORAL	LESIONAL	27
sub-HUP106	45	F	L	S	1B	RESECTION	ECOG	TEMPORAL	NON-LESIONAL	24
sub-HUP107	36	M	R	S	1A	RESECTION	ECOG	TEMPORAL	NON-LESIONAL	5
sub-HUP114	n/a	n/a	n/a	F	3A	ABLATION	ECOG	n/a	n/a	n/a
sub-HUP116	59	F	R	S	1A	ABLATION	SEEG	MTL	LESIONAL	42
sub-HUP123	n/a	n/a	n/a	S	1A	RESECTION	ECOG	n/a	n/a	n/a
sub-HUP126	n/a	n/a	n/a	S	1A	ABLATION	ECOG	n/a	n/a	n/a
sub-HUP130	46	F	L	S	1B	ABLATION	SEEG	MFL	NON-LESIONAL	20
sub-HUP134	n/a	n/a	n/a	S	1B	RESECTION	SEEG	n/a	n/a	n/a
sub-HUP135	37	M	R	F	2A	ABLATION	SEEG	MTL	NON-LESIONAL	34
sub-HUP138	38	M	L	F	4A	ABLATION	SEEG	MTL	LESIONAL	29
sub-HUP139	20	M	L	S	1A	ABLATION	SEEG	PARIETAL	LESIONAL	0
sub-HUP140	47	F	L	S	1B	ABLATION	SEEG	MTL	NON-LESIONAL	26
sub-HUP141	30	M	R	F	1C	ABLATION	SEEG	MTL	NON-LESIONAL	14
sub-HUP142	n/a	n/a	n/a	F	1D	ABLATION	SEEG	n/a	n/a	n/a
sub-HUP144	n/a	n/a	n/a	S	1D	RESECTION	SEEG	n/a	n/a	n/a
sub-HUP146	n/a	n/a	n/a	S	1A	RESECTION	SEEG	n/a	n/a	n/a
sub-HUP148	n/a	n/a	n/a	S	1A	ABLATION	SEEG	n/a	n/a	n/a
sub-HUP151	n/a	M	R	S	2A	ABLATION	SEEG	MFL	NON-LESIONAL	n/a
sub-HUP157	25	M	L	S	1B	ABLATION	SEEG	MTL	NON-LESIONAL	16
sub-HUP158	32	M	R	F	3A	ABLATION	SEEG	INSULAR	NON-LESIONAL	7
sub-HUP160	n/a	n/a	n/a	S	1A	RESECTION	SEEG	n/a	n/a	n/a
sub-HUP162	n/a	n/a	n/a	F	3A	ABLATION	SEEG	n/a	n/a	n/a
sub-HUP163	42	F	L	S	1D	ABLATION	SEEG	MTL	NON-LESIONAL	32
sub-HUP166	n/a	n/a	n/a	S	3A	RESECTION	SEEG	n/a	n/a	n/a
sub-HUP171	50	M	L	F	2A	ABLATION	SEEG	FRONTAL	NON-LESIONAL	6
sub-HUP177	42	F	R	S	1A	RESECTION	SEEG	TEMPORAL	NON-LESIONAL	5
sub-HUP187	n/a	n/a	n/a	S	2A	ABLATION	SEEG	n/a	n/a	n/a
sub-HUP190	25	M	L	F	3A	RESECTION	SEEG	MTL	NON-LESIONAL	12

2. Methods

2.1. Data selection

The dataset ds004100 [24], which pertained to epileptic seizures, was acquired from the OpenNeuro public database [21]. This dataset was obtained from the University of Pennsylvania Hospital and is accessible to researchers for public use [24]. We selected data of 39 patients (Table 1) from such public datasets. Due to the possibility of multiple seizures in the same patient, we selected data files from 104 seizures of these 39 patients, including 62 SEEG files and 42 ECOG files. Due to the fact that each seizure has three stages including Preictal, Ictal, and Postictal, we have extracted 20 s of data belonging to each stage from each data file in the following analysis. The University of Pennsylvania Hospital offers clinical markers for epileptic channels, in addition to the unprocessed data.

2.2. Data preprocessing

Sixty-two sEEG files and 42 ECoG files containing the seizure containing Preictal, Ictal, and Postictal periods of epilepsy patients were collected. Since the data was acquired from North America, we eliminated faulty electrodes and 60 Hz power frequency interference using the eeglab toolbox of the Matlab software [25]. The average signal was then employed as a point of reference when reassessing the iEEG data, while the baseline for each channel was eliminated. All data segments were resampled to 500 Hz. Each data segment was identified and extracted into three parts corresponding with three stages: before, during and after the epileptic seizure, each of which contained 20 s (10,000 sampling points) for alignment across different data segments with different length. The extraction of individual segment is shown in Fig. 3A.

2.3. Detrended fluctuation analysis (DFA) exponent

The DFA exponent measures the characteristic of long-range temporal correlation (LRTC), which reflects the patterns of neural activity with slow timescales and network's capability to store and process information over extended periods of time [16–18]. The calculation of the DFA exponent can be described as follows [18]: First, apply the Hilbert transform on the band-pass filtered data $d(k)$ to get the signal envelope as the amplitude $x(k)$, where k represents the time point. Then cumulatively summarize the average-removed amplitude $x(k)$ as $y(k)$:

$$x_{ave} = \frac{1}{N}\sum_{k=1}^{N} x(k) \tag{1}$$

$$y(k) = \sum_{i=1}^{k}[x(k) - x_{ave}] \tag{2}$$

Next, we define a series of window length Ls equidistantly distributed on the logarithmic scale; for each window length L in Ls, split $y(k)$ into non-overlapping fragments with length L and use the least square method to fit the local linear trend of each fragment:

$$y_n(k) = ak + b \tag{3}$$

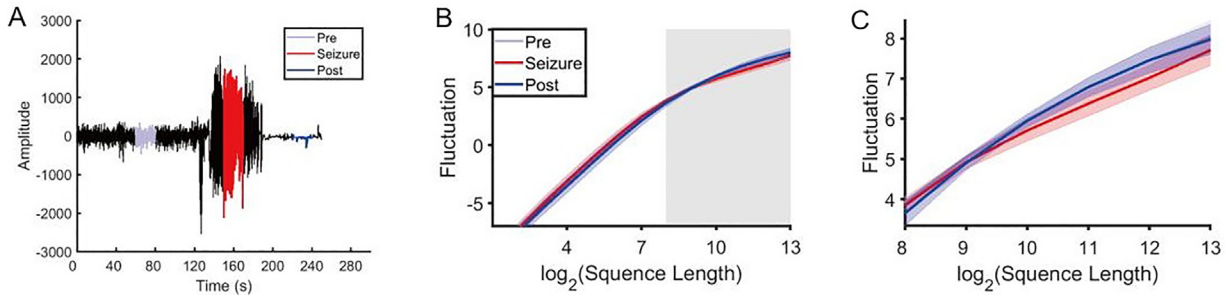

Fig. 3. Illustration of the DFA analysis. (A) Identification of different periods before, during and after the epileptic seizure, each of which contains 20 s segment. (B) illustration of F(L) corresponding with different L in the DFA analysis. DFA exponents were obtained from linear fits in double-logarithmic coordinates aver the depicted fitting range with linear relation as well as avoiding the influence of filters when estimating the exponent (gray range) [18]. (C) Enlargement of F(L) in the gray area in Fig. B.

In each time window, $y_n(k)$ was subtracted from the primary $y(k)$and the fluctuation function $F(L)$ was calculated as a squared deviation function defined as the average root mean square of the local-detrended cumulative amplitude.

$$F(L) = \sqrt{\frac{1}{N}\sum_{k=1}^{N}\left[y(k) - y_n(k)\right]^2} \tag{4}$$

$F(L)$ with all different window length L were then calculated. All values of $F(L)$ and L were transformed into a double-logarithmic coordinate and the least square method was used for estimating the linear trend between log($F(L)$) and log(L) to calculate the slope of the fitted line as the DFA exponent. The DFA exponent in different ranges indicates uncorrelated signal (DFA exponent > 1), long-scale correlated signal (0.5 < DFA exponent < 1) and anti-correlated signal (0 < DFA exponent < 0.5).

We calculated the DFA exponent on data fragments in sEEG and ECoG of single channel in 6 frequncy bands: broad (1–45 Hz) band, delta (1–4 Hz) band, theta (4–8 Hz) band, alpha (8–12 Hz) band, beta (12–30 Hz) band and gamma (30–45 Hz) band. Data was filtered to these bands using Hanning window and the 3-order zero-phase non-causal Butterworth filter. We defined L from 4 sampling points to 8,192 sampling points, equidistantly on a logarithmic scale based on 2. The DFA exponent was fitted on the log($F(L)$) with L ranging from 256 sampling points ($log(L) = 8$) to 8192 sampling points ($log(L) = 13$) that performed linear, satisfying the conditions for linear fitting and avoiding the influence of filter, as shown in Fig. 3B-C.

2.4. Classification

Then we classified the different stages before, during and after the epileptic seizure based on the features of DFA exponents in different bands. We tested three classification algorithms: Decision Tree (DT) model [26], Naive Bayesian (NB) model [27] and Linear Discriminant Analysis (LDA) model [28]. DT represents different possible outcomes and decision paths through a tree like decision-making process. At each node, the model selects the best splitting point based on the value of features, in order to divide the features into the most discriminative subsets. NB assumes that all features are independent of each other and classifies them by calculating the probability of features under each category, selecting the category with the highest probability as the final classification result. LDA finds a direction of projection that makes samples of the same category as close as possible and samples of different categories as far away as possible to achieve the good classification performance. The accomplishment of these three classification methods was based on the function in Matlab: *fitctree()* for DT, *fitcnb()* for NB and *fitcdiscr()* for LDA.

For training the classifier, we took DFA exponent in all of six bands (Broad band-Feature 1, Delta band-Feature 2, Theta band-Feature 3, Alpha band-Feature 4, Beta band-Feature 5, Gamma band-Feature 6) to construct the 1×6 feature sample. Three feature samples could be extracted for individual segment: one corresponding with the DFA exponent before the seizure, one corresponding with the DFA exponent during the seizure and one corresponding with the DFA exponent after the seizure. We randomly divided all samples among all segments into 80% training set and 20% testing set for 500 times. Classifier training was completed on the training set and the classification accuracy was examined on the testing set. We trained and tested the model in sEEG and ECoG separately. We examined the training time and memory required by the model. In addition, we alternately deleted one feature, with 1×5 feature vector left for the same classification task to determine which feature affected the performance of classification most, identifying the significant feature in distinguishing the different stages of epilepsy. Furthermore, we compared the classification performance using combination of DFA features with single DFA feature and classic feature used in the RNS system.

2.5. Slope of the power spectrum

The aperiodic properties in electrophysiological signals have been proved to be associated with various types of physiological states, such as cortical excitaion and inhibition (E/I) [29,30], age [31] and neurodegenerative diseases [32–34]. The aperiodic properties are embodied in the 1/f-like components of the power spectrum of the neural activity and can be measured by the slope of power spectrum. In this study we examined the slope of power spectrum in the low frequency band (1–15 Hz) and in the high frequency band (15–45 Hz), respectively. The slope was determined by linear fitting of the frequency and power in power spectrum under logarithmic coordinates [35,36].

$$log(Power) = klog(frequency) + b \tag{5}$$

where k was the slope of the power spectrum for further analysis.

2.6. Statistics

The comparisons of DFA exponent of each frequency band in either sEEG or ECoG were taken under three conditions: the DFA exponent before the seizure (Pre group) vs the DFA exponent during the seizure (Seizure group); the DFA exponent before the seizure (Pre group) vs the DFA exponent after the seizure (Post group); the DFA exponent during the seizure (Seizure group) vs the DFA exponent after the seizure (Post group). The comparisons of slope of the low frequency band or the high frequency band were taken under these conditions mentioned above too. When identifying the key feature for classification, post-hoc comparison was taken between the accuracy using all features and the accuracy with feature 1 (broad band DFA exponent) deleted of each model. Two-sides paired t-test was applied on each comparison. All significances were judged as P-value < 0.05 after Bonferroni correction.

The Pearson correlation coefficient and their significance between broad band DFA exponent and the slope in the low frequency band or the high frequency band were tested. The significances of the correlation were judged as P-value < 0.05.

3. Results

3.1. Overview of research contents

During the process of signal analysis, the signals obtained from each channel are extracted individually for examination. Subsequently, the corresponding indicators for all channels are tallied. (1) An intuitive analysis reveals that the signal exhibits discernible fluctuations throughout the pre-ictal, ictal, and post-ictal phases (Fig. 3A). To differentiate between distinct characteristics, we employ the DFA exponent as an indicator and utilize numeric values to compare the differences of this indicator across three phases. (2) Given that SEEG and ECoG represent distinct classifications of electrical stimulation systems (rDBS and rFCS, respectively), and that epilepsy signals may exhibit variations in characteristics across frequency bands, we partitioned all data into six local groups (1–45 Hz, 1–4 Hz, 4–8 Hz, 8–12 Hz, 12–30 Hz, and 30–45 Hz) for the purpose of conducting distinct analyses and statistics. (3) To determine whether this indicator can function as an intermediary variable for machine learning-based automatic classification algorithms, we classified the three phases in 312 samples out of 104 data segments using methods including Decision Tree (DT) model, Naive Bayesian (NB) model, and Linear Discriminant Analysis (LDA) model. We then compared the training results obtained using various simple machine learning models. (4) Finally, to further assess the interpretability of DFA exponents as a characteristic of neural signals, we applied the grouping method described in the second step to Power Spectrum Slope Analysis (PSSA) on all data and statistically analyzed the linear correlation between the labels derived from PSSA and those derived from DFA exponents.

3.2. Intermediary variables between data and condition triggers

The DFA exponent quantifies the attributes of Long Term Time Correlation (LRTC), a metric that signifies the capacity of a neural network to retain and process information for extended durations and corresponds to patterns of neural activity that occur over slow time scales [16–18]. In the methodology section, a comprehensive account of the calculation method and mathematical formula utilized to derive this exponent has been furnished (Fig. 3). The six-element array [DFA - broad band, DFA - delta band, DFA - theta band, DFA - alpha band, DFA - beta band, DFA - gamma band] will serve as the intermediate variable between the data and the triggering condition and as the input variable for machine learning models. By designating the array samples as the pre-ictal, ictal and post-ictal periods, respectively, and training them with models including Decision Tree model, Naive Bayesian model, and linear discriminant Analysis model, we will accomplish the automated classification of the test set. While our objective is to decrease the computational demands of the system through the incorporation of intermediate variables, it remains imperative to validate the ultimate accuracy that can be attained with this approach.

3.3. Performance of DFA exponent

First we analyzed the change of DFA exponent in sEEG and ECoG at six frequency bands: broad band (1–45 Hz), delta band (1–4 Hz), theta band (4–8 Hz), alpha band (8–12 Hz), beta band (12–30 Hz), gamma band (30–45 Hz). The single-channel DFA exponent of these six bands before, during and after the epileptic seizure in sEEG of one individual segment is shown in Fig. 4.

The result of DFA exponent in sEEG is shown in Fig. 5. The DFA exponent exhibited various patterns of change at different frequency bands. Specifically, the DFA exponent during the epileptic seizure was lower compared with the DFA exponent before and after the epileptic seizure, while the DFA exponent before the epileptic seizure was lower compared with the DFA exponent after the epileptic seizure at broad band (Fig. 5A; Pre vs Seizure, $p < 0.001$; Post vs Seizure, $p < 0.001$; Pre vs Post, $p < 0.05$; Bonferroni corrected) and delta band (Fig. 5B; Pre vs Seizure, $p < 0.001$; Post vs Seizure, $p < 0.001$; Pre vs Post, $p < 0.01$; Bonferroni corrected). Different from the changes in aforementioned frequency bands, both the DFA exponent during and after the epileptic seizure was lower than the DFA exponent before the epileptic seizure at theta band (Fig. 5C; Pre vs Seizure, $p < 0.01$; Pre vs Post, $p < 0.001$; Bonferroni corrected), alpha band (Fig. 5D; Pre vs Seizure, $p < 0.01$; Pre vs Post, $p < 0.001$; Bonferroni corrected) and beta band (Fig. 5E; Pre vs Seizure, $p < 0.001$; Pre vs Post, $p < 0.01$; Bonferroni corrected). In gamma band, the DFA exponent before the epileptic seizure was lower than the DFA exponent after the epileptic seizure (Fig. 5F; Pre vs Post, $p < 0.05$; Bonferroni corrected).

The result of DFA exponent in ECoG is shown in Fig. 6. The DFA exponent showed different patterns of change at distinct frequency bands too, but these changes at each band were different from those in sEEG. The DFA exponent during the epileptic seizure was lower than the DFA exponent before the epileptic seizure at broad band (Fig. 6A; Pre vs Seizure, $p < 0.001$; Bonferroni corrected). Conversely, The DFA exponent during the epileptic seizure was higher than the DFA exponent before and after the epileptic seizure at theta band (Fig. 6C; Pre vs Seizure, $p < 0.001$; Post vs Seizure, $p < 0.001$; Bonferroni corrected) and alpha band (Fig. 6D; Pre vs Seizure, $p < 0.001$; Post vs Seizure, $p < 0.001$; Bonferroni corrected). In other frequency bands, the DFA exponent didn't show significant change before, during and after the epileptic seizure (Delta band, Fig. 6B; Beta band, Fig. 6E; Gamma band, Fig. 6F; Bonferroni corrected).

In conclusion, the change of DFA exponent was complicated across different frequency bands, as well as exhibited different patterns between deep activities with sEEG and cortical activities with ECoG. These results suggested the complexity of dynamic variation corresponding with LRTC within the epilepsy network.

3.4. Performance of machine learning models

Next we tried to classify the different stages before, during and after the epileptic seizure and identify the key feature among the DFA exponent in different bands. The results of classifying different stages of epilepsy (before, during and after the epileptic seizure) measured by classification accuracy on the test datasets are shown in Fig. 7. The results of classification in sEEG are shown in Fig. 7A-C (Fig. 7A, DT; Fig. 7B, NB; Fig. 7C, LDA). The results of classification in ECoG are shown in Fig. 7D-F (Fig. 7D, DT; Fig. 7E, NB; Fig. 7F, LDA). All of the test accuracy with all features or one feature deleted were higher than the random level (0.33, black dashed line), demonstrating the sufficient capability of DFA exponent characterizing the different stages of epilepsy. Furthermore, when the Feature 1 (Broad band DFA exponent) was deleted, the accuracy showed the most significant decline compared with deleting other features among all conditions, indicating the significant role of broad-band DFA exponent in distinguishing the different stages of epilepsy.

We compared the performances among classification algorithms from three aspects: classification accuracy, time for training classifier and memory for classifier. The results of classifying in sEEG are shown in Table 2 (Classification accuracy, Table 2-1; Time for training classifier, Table 2-2; Memory for classifier, Table 2-3). In detail, the classification accuracy of LDA was higher than DT and NB, while the performances of DT and NB were similar; DT took longer than LDA and LDA took longer than NB for training the classifier; LDA occupied more memory than DT and DT occupied more memory than NB for storage. The results of classifying in ECoG are shown in Table 3 (Classification accuracy, Table 3-1; Time for training classifier, Table 3-2; Memory for classifier, Table 3-3).

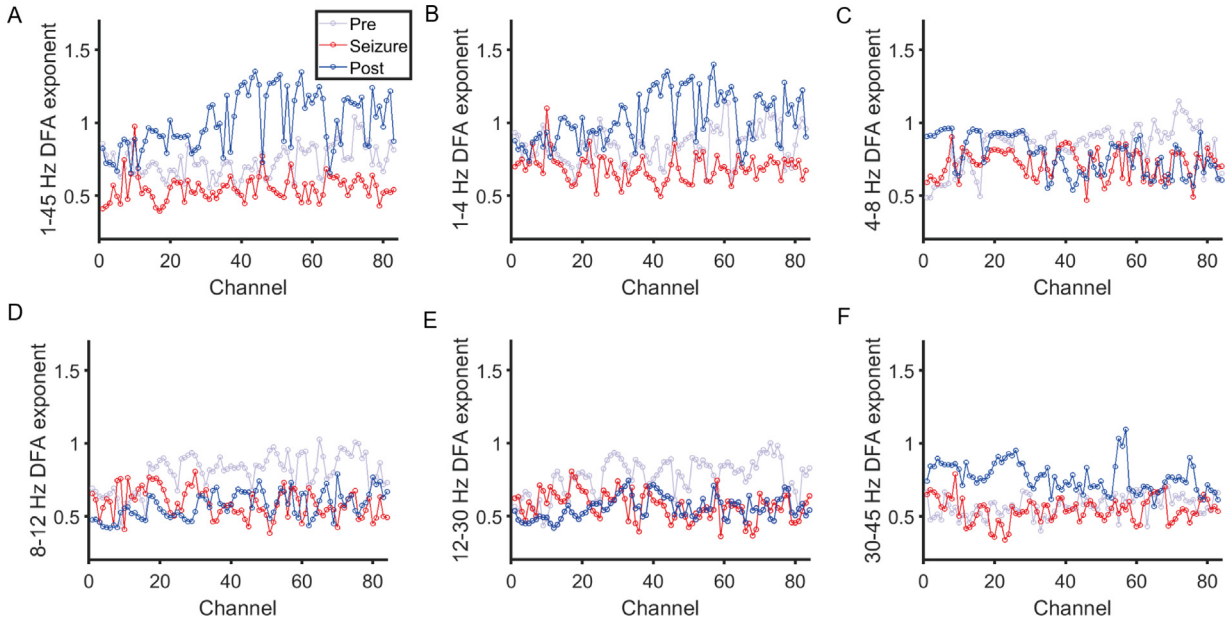

Fig. 4. Single channel DFA exponent of one individual segment in sEEG. (A) Broad (1–45 Hz) band. (B) Delta (1–4 Hz) band. (C) Theta (4–8 Hz) band. (D) Alpha (8–12 Hz) band. (E) Beta (12–30 Hz) band. (F) Gamma (30–45 Hz) band. The shallow gray, red and blue curve indicated the single-channel DFA exponent in the preictal, ictal and postictal period, respectively.

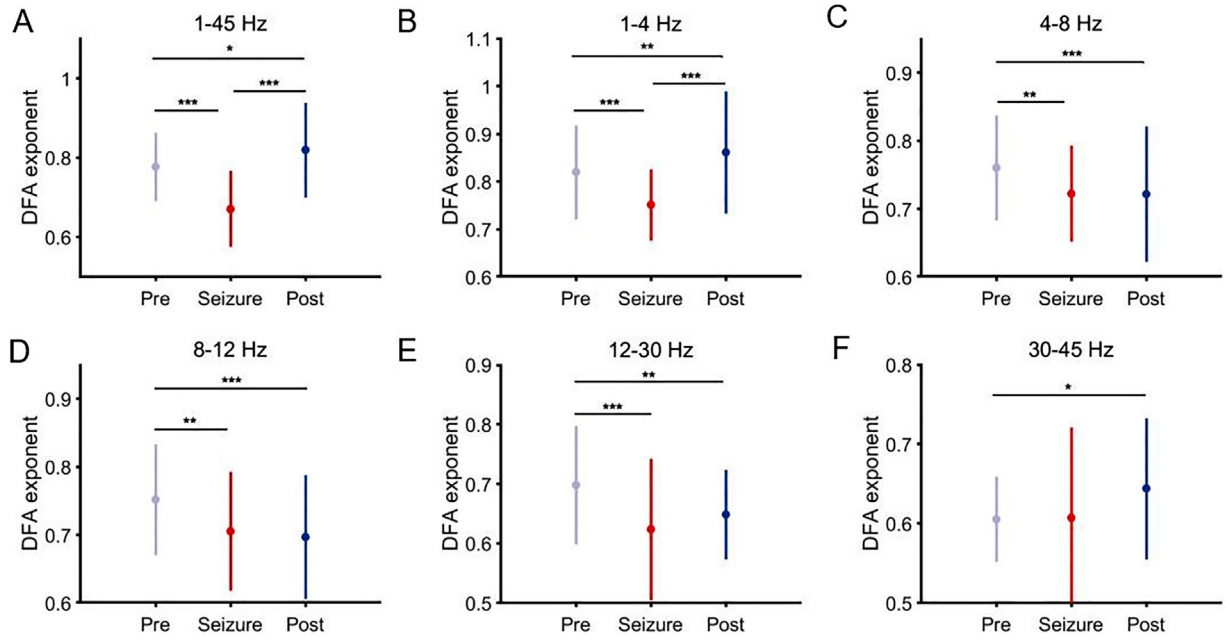

Fig. 5. Change of DFA exponent in different frequency bands before, during and after the epileptic seizure in sEEG data. (A) Broad (1–45 Hz) band. (B) Delta (1–4 Hz) band. (C) Theta (4–8 Hz) band. (D) Alpha (8–12 Hz) band. (E) Beta (12–30 Hz) band. (F) Gamma (30–45 Hz) band. $^{*}p < 0.05$, $^{**}p < 0.01$, $^{***}p < 0.001$; Two-sides paired *t*-test after Bonferroni corrected. Error bar represents SEM.

Table 2–1
Classification accuracy.

	All Features	Delete Feature 1	Delete Feature 2	Delete Feature 3	Delete Feature 4	Delete Feature 5	Delete Feature 6
Decision Tree	0.57 ± 0.07	0.54 ± 0.08	0.57 ± 0.07	0.58 ± 0.07	0.58 ± 0.08	0.57 ± 0.07	0.59 ± 0.08
Naive Baysesian	0.59 ± 0.08	0.53 ± 0.08	0.63 ± 0.07	0.61 ± 0.08	0.58 ± 0.08	0.55 ± 0.08	0.59 ± 0.08
Linear Discriminant Analysis	0.67 ± 0.07	0.65 ± 0.08	0.67 ± 0.07	0.67 ± 0.07	0.67 ± 0.07	0.65 ± 0.07	0.64 ± 0.07

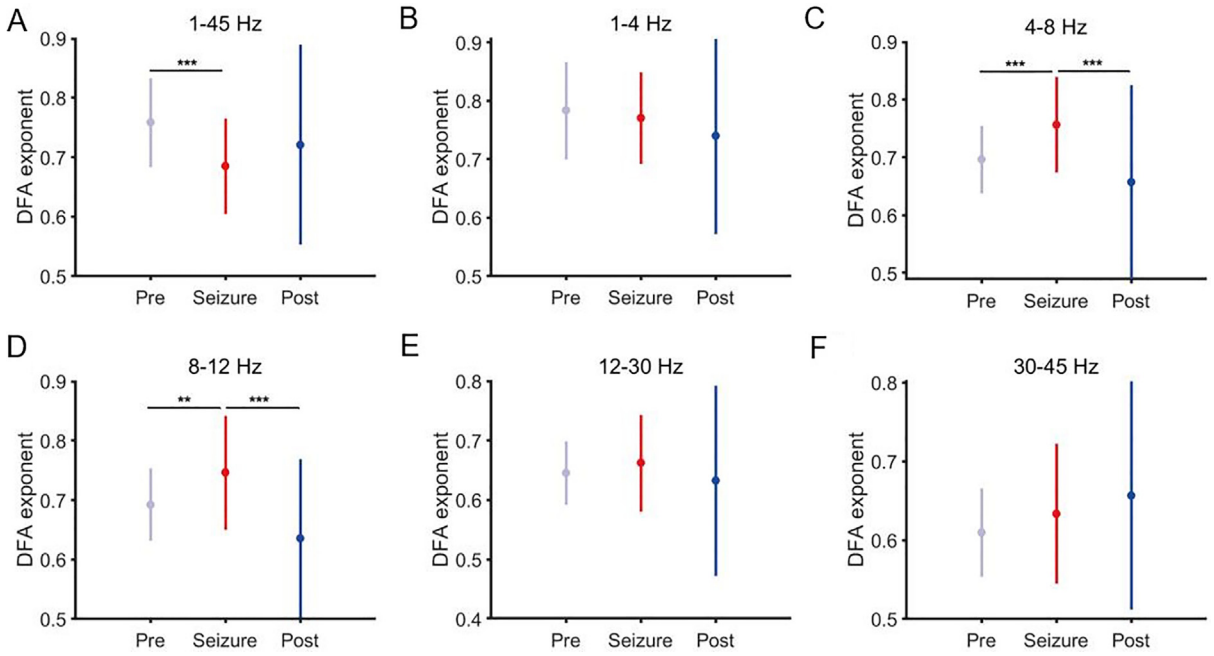

Fig. 6. Change of DFA exponent in different frequency bands before, during and after the epileptic seizure in ECoG data. (A) Broad (1–45 Hz) band. (B) Delta (1–4 Hz) band. (C) Theta (4–8 Hz) band. (D) Alpha (8–12 Hz) band. (E) Beta (12–30 Hz) band. (F) Gamma (30–45 Hz) band. $^{*}p < 0.05$, $^{**}p < 0.01$, $^{***}p < 0.001$; Two-sides paired *t*-test after Bonferroni corrected. Error bar represents SEM.

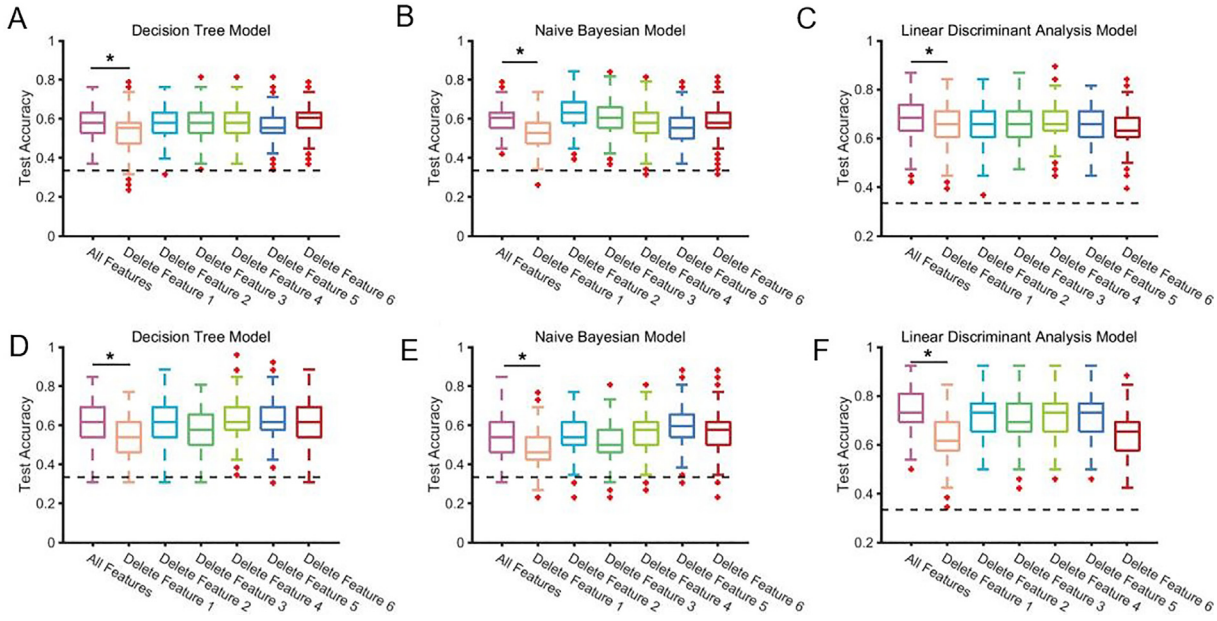

Fig. 7. Classification accuracy. (A) Decision Tree (DT) model in sEEG data. (B) Naive Bayesian (NB) model in sEEG data. (C) Linear discriminant analysis (LDA) model in sEEG data. (D) DT model in ECoG data. (E) NB model in ECoG data. (F) LDA model in ECoG data. Post-hoc comparison between the accuracy with all features and the accuracy with feature 1 (broad band DFA exponent) deleted was taken. $^{*}p < 0.05$; Two-sides paired *t*-test after Bonferroni corrected.

Table 2–2
Time for training classifier (ms).

	All Features	Delete Feature 1	Delete Feature 2	Delete Feature 3	Delete Feature 4	Delete Feature 5	Delete Feature 6
Decision Tree	2.79 ± 0.55	2.77 ± 0.69	2.76 ± 0.63	2.77 ± 0.58	2.88 ± 0.70	2.86 ± 0.62	2.83 ± 0.55
Naive Baysesian	1.89 ± 0.47	1.83 ± 0.29	1.80 ± 0.19	1.73 ± 0.07	1.71 ± 0.08	1.71 ± 0.06	1.77 ± 0.11
Linear Discriminant Analysis	2.50 ± 1.14	2.42 ± 0.34	2.70 ± 0.57	2.53 ± 0.53	2.64 ± 0.61	3.02 ± 1.83	2.50 ± 0.38

Table 2–3
Memory for classifier (kb).

	All Features	Delete Feature 1	Delete Feature 2	Delete Feature 3	Delete Feature 4	Delete Feature 5	Delete Feature 6
Decision Tree	139.12 ± 5.03	135.51 ± 4.87	130.07 ± 5.52	130.35 ± 4.92	129.77 ± 5.38	130.30 ± 5.07	132.05 ± 4.82
Naive Baysesian	125.32 ± 0	111.98 ± 0	111.98 ± 0	111.98 ± 0	111.98 ± 0	111.98 ± 0	111.98 ± 0
Linear Discriminant Analysis	148.02 ± 0	136.15 ± 0	136.15 ± 0	136.15 ± 0	136.15 ± 0	136.15 ± 0	136.15 ± 0

Table 3–1
Classification accuracy.

	All Features	Delete Feature 1	Delete Feature 2	Delete Feature 3	Delete Feature 4	Delete Feature 5	Delete Feature 6
Decision Tree	0.61 ± 0.09	0.54 ± 0.09	0.62 ± 0.09	0.58 ± 0.09	0.62 ± 0.10	0.62 ± 0.09	0.61 ± 0.10
Naive Baysesian	0.55 ± 0.10	0.48 ± 0.08	0.54 ± 0.10	0.51 ± 0.09	0.56 ± 0.09	0.59 ± 0.09	0.57 ± 0.10
Linear Discriminant Analysis	0.73 ± 0.08	0.62 ± 0.09	0.73 ± 0.08	0.69 ± 0.08	0.72 ± 0.08	0.72 ± 0.08	0.64 ± 0.08

Table 3–2
Time for training classifier (ms).

	All Features	Delete Feature 1	Delete Feature 2	Delete Feature 3	Delete Feature 4	Delete Feature 5	Delete Feature 6
Decision Tree	2.38 ± 0.39	2.58 ± 0.50	2.35 ± 0.46	2.74 ± 0.71	2.77 ± 0.44	2.34 ± 0.47	2.28 ± 0.43
Naive Baysesian	1.87 ± 0.20	1.83 ± 0.24	1.74 ± 0.13	1.75 ± 0.14	1.74 ± 0.09	1.75 ± 0.10	1.71 ± 0.07
Linear Discriminant Analysis	2.71 ± 0.63	2.37 ± 0.34	2.42 ± 0.37	2.37 ± 0.37	2.34 ± 0.28	2.36 ± 0.38	2.42 ± 0.32

Table 3–3
Memory for classifier (kb).

	All Features	Delete Feature 1	Delete Feature 2	Delete Feature 3	Delete Feature 4	Delete Feature 5	Delete Feature 6
Decision Tree	102.19 ± 4.02	101.54 ± 4.08	95.86 ± 3.88	96.59 ± 4.06	97.99 ± 4.47	96.15 ± 4.10	96.51 ± 3.56
Naive Baysesian	98.32 ± 0	87.98 ± 0	87.98 ± 0	87.98 ± 0	87.98 ± 0	87.98 ± 0	87.98 ± 0
Linear Discriminant Analysis	124.02 ± 0	115.15 ± 0	115.15 ± 0	115.15 ± 0	115.15 ± 0	115.15 ± 0	115.15 ± 0

Table 4–1
Classification accuracy with RNS feature of sEEG.

	Line Length	Area	Bandpass
Decision Tree	0.67 ± 0.07	0.54 ± 0.07	0.58 ± 0.07
Naive Baysesian	0.54 ± 0.07	0.37 ± 0.07	0.64 ± 0.07
Linear Discriminant Analysis	0.47 ± 0.06	0.33 ± 0.08	0.61 ± 0.07

Table 4–2
Classification accuracy with RNS feature of ECoG.

	Line Length	Area	Bandpass
Decision Tree	0.58 ± 0.09	0.56 ± 0.09	0.52 ± 0.08
Naive Baysesian	0.54 ± 0.08	0.36 ± 0.08	0.57 ± 0.09
Linear Discriminant Analysis	0.50 ± 0.09	0.45 ± 0.09	0.56 ± 0.08

Specifically, the classification accuracy of LDA was higher than DT, and the accuracy of DT was higher than NB; LDA spent comparable time with DT, longer than NB for training the classifier; Similar with the performances in sEEG, LDA occupied more memory than DT, as well as DT occupied more memory than NB for storage. Furthermore, the classification performance of combination of multiple DFA features was higher than the performance of feature used in the RNS system (Table 4) or the single (Table 4-2, Table 5-2) DFA feature (Table 5), suggesting the significance of feature combination.

Overall, LDA had the highest classification accuracy among all of three algorithms. NB had the lowest classification accuracy, but it required the shortest training time and least storage assumption.When using them in practice, various factors evaluating the algorithm performances should be comprehensively considered.

3.5. Slope analysis of power spectrum

In addition, we considered the slope of the power spectrum corresponding with the aperiodic or the 1/f-like components of the neural activity. Here we analyzed the slope of the low frequency range (1–15 Hz) and the high frequency range (15–45 Hz), respectively. The results of the slope analysis are shown in Fig. 8.

The power spectrum of neural activity before, during and after the epileptic seizure in sEEG is shown in Fig. 8A, following the comparison of slope in the low frequency range shown in Fig. 8B and high frequency range in Fig. 8C. In the low frequency range, the slope during the epileptic seizure was higher than the slope before and after the epileptic seizure, and the slope before the epileptic seizure was higher than the slope after the epileptic seizure (Fig. 8B; Pre vs Seizure, $p < 0.001$; Post vs Seizure, $p < 0.001$; Pre vs Post, $p < 0.001$; Bonferroni corrected). Conversely, in the high frequency band, the slope during the epileptic seizure was lower than the slope before and after the epileptic seizure, and the slope before the epileptic seizure was lower than the slope after the epileptic seizure (Fig. 8C; Pre vs Seizure, $p < 0.001$; Post vs Seizure, $p < 0.001$; Pre vs Post, $p < 0.001$; Bonferroni corrected).

The power spectrum of neural activity before, during and after the epileptic seizure in ECoG is shown in Fig. 8D, following the comparison of slope in the low frequency range shown in Fig. 8E and high frequency range in Fig. 8F. Similar with the results in sEEG, the slope during the epileptic seizure was higher than the slope before and after the epileptic seizure, and the slope before the epileptic seizure was higher than the slope after the epileptic seizure in the low frequency (Fig. 8E; Pre vs Seizure, $p < 0.001$; Post vs Seizure, $p < 0.001$; Pre vs Post, $p < 0.001$; Bonferroni corrected). Opposite to the low frequency band, the slope during the epileptic seizure was lower than the slope before and after the epileptic seizure, and the slope before the epileptic seizure was lower than the slope after the epileptic seizure in the high frequency. (Fig. 8F;

Table 5–1
Classification accuracy with single DFA feature of sEEG.

	Feature 1	Feature 2	Feature 3	Feature 4	Feature 5	Feature 6
Decision Tree	0.49 ± 0.07	0.43 ± 0.08	0.40 ± 0.07	0.32 ± 0.06	0.44 ± 0.07	0.35 ± 0.07
Naive Baysesian	0.53 ± 0.07	0.46 ± 0.07	0.41 ± 0.08	0.40 ± 0.07	0.43 ± 0.08	0.44 ± 0.08
Linear Discriminant Analysis	0.54 ± 0.08	0.43 ± 0.07	0.36 ± 0.07	0.39 ± 0.07	0.42 ± 0.08	0.35 ± 0.07

Table 5–2
Classification accuracy with single DFA feature of ECoG.

	Feature 1	Feature 2	Feature 3	Feature 4	Feature 5	Feature 6
Decision Tree	0.40 ± 0.09	0.33 ± 0.08	0.48 ± 0.09	0.48 ± 0.09	0.34 ± 0.08	0.37 ± 0.09
Naive Baysesian	0.46 ± 0.09	0.36 ± 0.09	0.48 ± 0.09	0.50 ± 0.10	0.43 ± 0.09	0.40 ± 0.09
Linear Discriminant Analysis	0.37 ± 0.09	0.29 ± 0.08	0.44 ± 0.09	0.49 ± 0.10	0.30 ± 0.08	0.33 ± 0.09

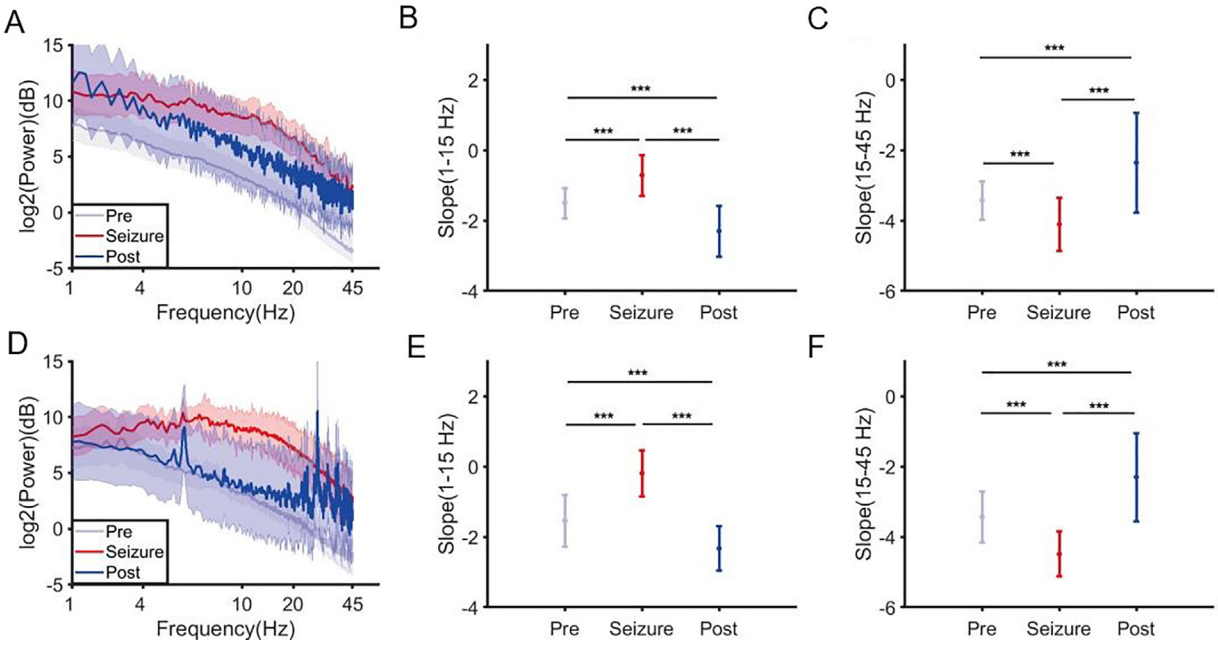

Fig. 8. Slope of power spectrum before, during and after the epileptic seizure. (A) Power spectrum in sEEG. (B) Comparison of slope in the low frequency band (1–15 Hz) in sEEG. (C) Comparison of slope in the high frequency band (15–45 Hz) in sEEG. (D) Power spectrum in ECoG. (E) Comparison of slope in the low frequency band (1–15 Hz) in ECoG. (F) Comparison of slope in the high frequency band (15–45 Hz) in ECoG. $^{***}p < 0.001$; Two-sides paired *t*-test after Bonferroni corrected. Error bar represents SEM.

Pre vs Seizure, $p < 0.001$; Post vs Seizure, $p < 0.001$; Pre vs Post, $p < 0.001$; Bonferroni corrected).

Furthermore, we examined the relationship between the slope of power spectrum and DFA exponent in Fig. 9. The correlation between the broad-band DFA exponent and the slope in the low frequency band as well as the high frequency band in sEEG is shown in Fig. 9A and B, respectively. The broad-band DFA exponent was negatively correlated with the slope in the low frequency band (Fig. 9A, $r = -0.54$, $p < 0.001$), while was positively correlated with the slope in the high frequency band (Fig. 9B, $r = 0.33$, $p < 0.001$). The correlation between the broad-band DFA exponent and the slope in the low frequency band as well as the high frequency band in ECoG is shown in Fig. 9C and 9D, respectively, both of which didn't reach the significant level (Fig. 9C, $r = -0.12$, $p = 0.16$; Fig. 9D, $r = 0.05$, $p = 0.58$).

4. Discussion

4.1. Performance requirements for feedback circuits

Ever since the inception of bioelectronic device development, energy provision and safety concerns have been formidable obstacles. While wireless charging technology has been employed in clinical trials and scientific research pertaining to specific implantable medical devices, it is still advantageous for patients to minimize the frequency of charges in terms of energy provision. Heat generation, volume, and biocompatibility are all factors that electronic device developers must take into account with regard to security [37,38]. Circuit-related concerns primarily encompass heat generation and volume. The optimization of power consumption and volume has emerged as a viable strategy to contemplate. When considering algorithm design, a design solution that reduces both algorithm complexity and data complexity can concurrently alleviate the power consumption and volume constraints by lowering the computational performance requirements of the chip and the storage performance requirements of the disk. The long-term autocorrelation coefficient is employed as an intermediary variable in the training of machine learning models in this article. The utilization of the long-term autocorrelation index in conjunction with a six-element array simplifies the algorithm complexity necessary for traditional algorithms or direct training of raw data, while still accurately representing the critical states of epileptic electroencephalography. By decreasing the volume of training sets that require to be seared into the feedback type electrical stimulation system, electronic device safety was ensured.

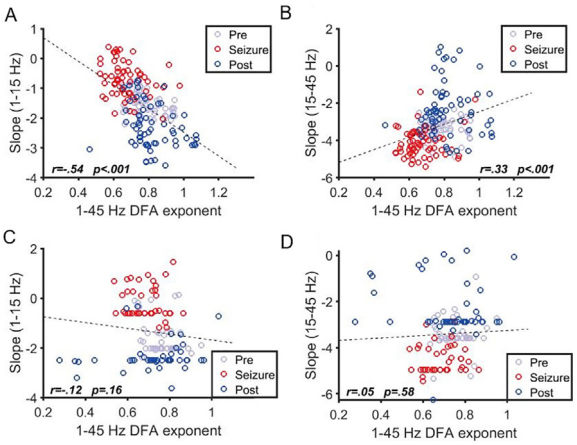

Fig. 9. Correlation between broad-band DFA exponent and slope of power spectrum. (A) Correlation between broad-band DFA exponent and slope in the low frequency band in sEEG. (B) Correlation between broad-band DFA exponent and slope in the high frequency band in sEEG. (C) Correlation between broad-band DFA exponent and slope in the low frequency band in ECoG. (D) Correlation between broad-band DFA exponent and slope in the high frequency band in ECoG.

4.2. Comparison between rDBS and rFCS

In light of the fact that RNS can be subdivided into rDBS and rFCS, the data types of SEEG and ECoG must be discussed separately. Based on the evaluation outcomes of the machine learning model, it is evident that the ECoG model exhibits superior performance in comparison to the SEEG model. This disparity may indicate that feedback cortical stimulation is a more appropriate approach for managing focal cortical lesions. In fact, the Slope Analysis of the Power Spectrum might have provided confirmation of this phenomenon. Our charts indicate that the Power Spectral Slope of ECoG data exhibits greater variation across distinct seizure states. Furthermore, the ECoG curve undergoes substantial fluctuations at approximately 4 Hz and 30 Hz. The findings of this study indicate that the signal properties of ECoG might be more appropriate for identifying feedback triggering conditions. Moreover, these distinctions entirely demonstrate the need to divide RNS into two distinct categories—rDBS and rFCS—and to train the data independently, even in the absence of any evaluation of the training outcomes produced by the two data types' superiority or inferiority.

4.3. Algorithm design of feedback trigger

Following a discussion of the efficacy of DFA exponents in describing epileptic states, the outcomes of training a simple machine learning model with DFA exponents as intermediate variables are presented in this article. When attempting to define the epileptic state, DFA exponent of neural signal can be likened to the speed of a small ball. During the post phase of the ictal, the diminutive ball is positioned atop the mountain, possessing the least amount of kinetic energy and the slowest velocity. The small ball descends to the precipice, gains kinetic energy, and accelerates in velocity as time passes. The moment the epileptic seizure commences, the diminutive ball descends towards the ground at its maximum velocities and kinetic energies. The ball returned along the ascent to the mountain peak subsequent to the seizure, where its kinetic energy underwent a conversion back into gravitational potential energy. The utilization of DFA exponent permits the organic division of distinct critical states of neural activity. These states can be utilized as a prerequisite for commencing electrical stimulation or incorporated into the algorithm that automatically activates feedback triggers. To validate the viability of this algorithm for automatic triggering, we performed preliminary research on automatic classification methods based on intermediate variables using three simple machine learning models on randomly partitioned datasets: the Decision Tree model, the Naive Bayesian model, and the Linear Discriminant Analysis model. We have not yet extended machine learning methods to deep neural network models [39] and generative neural network models [40], despite our limited knowledge and expertise in this area. Nonetheless, the optimization of classification accuracy through the utilization of deep learning and generative learning will continue to be a subject of interest in future research for quite some time.

4.4. Significance of this investigation

Before proceeding, this article divides RNS into two categories based on the stimulation targets: rDBS and rFCS. Future research will be able to characterize the various types of intracranial electrical stimulators with greater precision thanks to this classification. Furthermore, classifying signals according to their distinct characteristics, such as SEEG and ECoG, is also imperative. We earnestly request that scholars from other research organizations adopt our refined classification system as a means to mitigate perplexity and uncertainty inherent in the paper's description. The second step was to feed the machine learning model an array of DFA exponents as intermediate variables, thereby validating the viability of this machine learning method via intermediate variables. As a result of DFA exponent's biological correlation, the machine learning model we developed possesses excellent biological interpretability. In the interim, the utilization of intermediate variables for training purposes obviates the necessity to input the enormous amounts of data acquired from intracranial electrophysiological monitoring into intricate models or machine learning frameworks. By significantly diminishing the computational and storage demands of the system, this methodology effectively contributes to the assurance of implanted device safety. Methods and evidence are presented to support the use of DFA exponents in feedback electrical stimulation systems. Additionally, the concept of training models using intermediate variables is elaborated upon.

4.5. Neurobiological challenges faced by feedback based electrical stimulation systems

As discussed in this article, the DFA exponent and the logarithmic spectral slope are only indicative of specific characteristics of an epileptic data; the neurobiological principles underlying these characteristics remain unknown to researchers [41]. The neural activity mechanisms that result in a sustained reduction in long-range temporal correlation of signal features in seizure phases remain unclear to the public. Simultaneously, the issue of neural modulation and the cessation of seizures in epilepsy patients in response to a specific frequency band of electrical stimulation remains obscure [42], as does the mechanism underlying the alleviation or resolution of tremors and neurodegeneration in Parkinson's patients. The neurobiological principles underlying epileptic seizures remain obscure, as does the rationale behind the efficacy of specific frequency bands of electrical stimulation in the treatment of neurological and psychiatric disorders. In most cases, post-validation is required to demonstrate the efficacy of a particular neural recording or modulation technique; this validation may be merely statistically significant and not physiologically significant. Nevertheless, after numerous iterations across the annals of humankind, deep brain stimulation has emerged as the preeminent therapeutic approach for Parkinson's disease. Despite the lack of clarity surrounding feedback-based electrical stimulation, there remains optimism that such systems may one day contribute to the resolution of epilepsy issues in humans.

4.6. Future prospects and constraints of this research

Already mentioned in the preceding section are the deficiencies and drawbacks of this article. Due to our lack of familiarity with the training methods of deep neural network models and generative neural net-

work models, the greatest flaw of this article is that we did not use the six-element array trained and tested in previous three models for these models. However, we are well aware of the enormous classification accuracy potential of deep neural network models and generative neural network models. Nevertheless, the argument put forth in this article remains valid, and the utilization of DFA exponent to automatically classify the critical state of epilepsy is effective. As is observed, the change of broad-band (1–45 Hz) DFA exponent was similar across different periods in both sEEG and ECoG, suggesting the overall variation of network E/I before, during and after the seizure. In detail, the DFA exponent during the seizure was lower than the DFA exponent before and after the seizure, indicating the more serious breakdown of network E/I balance during the epilepsy seizure. After the seizure, the DFA exponent increased corresponding with the recovery of E/I balance of the brain network. Utilizing DFA exponents as intermediate variables during training in three simple machine learning models can significantly reduce the storage and computational demands of feedback-based electrical stimulation systems while maintaining a high level of classification accuracy. This has the potential to yield significant benefits for patients. The lack of clarity regarding the neurobiological principles underlying the DFA exponent is an additional shortcoming of this article, as it obscures crucial prior knowledge. Nevertheless, the efficacy of the DFA exponent as a biomarker suffices to justify its application in the development of feedback electrical stimulation systems. As a result, our objectives for forthcoming investigations are twofold: firstly, to employ DFA exponent in the training process of deep neural network models or generative neural network models; and secondly, to conduct biological experiments that elucidate the fundamental biological principles underlying the long-range temporal correlation.

5. Conclusion and implications

Numerous studies have demonstrated that electrical stimulation has an improvement effect on various neurological and psychiatric disorders. Especially in the field of Parkinson's disease, deep brain stimulation has become a prominent field of treatment. Early electrical stimulation was open-loop, and doctors only needed to place the electrode connecting the wire directly on the target nucleus and regulate them according to fixed stimulation parameters. Later, researchers found that from the perspective of electrophysiological signals, Parkinson's disease usually manifests as abnormalities in the Beta frequency band [43]. Dynamically adjusting stimulation parameters based on the signal characteristics of the Beta frequency band may further improve treatment effectiveness, such as further enhancing the patient's motor precision. Therefore, dynamically adjusting stimulus parameters, from open loop to closed loop, has become a major background in the field of neural regulation.

The mechanism of each neurological and psychiatric disease is different, so the treatment plans for different diseases are also different. Epilepsy is usually a internal disorder, in which patients take medications such as levetiracetam, lamotrigine, carbamazepine, and sodium valproate to alleviate seizure frequency and symptoms. But about one-third of patients could not be cured through medication [44], especially for temporal lobe and hippocampal epilepsy, and 80% of patients are drug-resistant in such two types. For patients with drug-resistant nature, resection of cortical lesions and thermal coagulation of deep lesions have become common surgical treatments. However, there are some lesions that could not be destroyed, such as the hardened bilateral hippocampus. If both hippocampus are destroyed simultaneously, patients will lose their long-term memory ability forever. Therefore, for these special epilepsy patients, electrical stimulation seems to be the only optional choice. However, even with the use of electrical stimulation as a treatment option, the situation of epilepsy is different from that of Parkinson's disease, and the electrophysiological signal characteristics and electrical stimulation targets of these two diseases are completely different.

The lesions and circuits of Parkinson's disease are clear, while the lesions of epilepsy are highly individualized, as if any lump of brain tissue could become the source of epilepsy. Therefore, in the field of epileptic electrical stimulation, there have always been two different sounds. The first sound is to ignore the issue of individualized lesions and uniformly stimulate the thalamus [2,22] as the center of the Papez circuit. The second sound is that since the lesion is highly individualized, we stimulate it wherever it is. The stimulation parameters for different targets are similar, but the biomarkers for identifying seizure status are different. However, regardless of which sound is correct, the significance of automatically identifying seizure status is that although open-loop electrical stimulation according to fixed stimulus parameters seems to alleviate seizure frequency and symptoms, could we block this seizure if we perform electrical stimulation or adjust stimulus parameters when it is about to occur? If we perform electrical stimulation or adjust stimulation parameters when the seizure has already begun, could we alleviate this seizure or make it end faster? These scientific questions constitute the demand for closed-loop neural regulation in the field of epilepsy, so we need to use automated methods to enable machines to understand when patients are about to have seizures and when they are currently having seizures.

Therefore, our research has clear implications for clinical practice. The important role of biomarkers and machine learning models in neural electrical stimulation or other treatment options is that they enable machines to understand human instructions and automate their execution. Machines are accurate and precise, as doctors may fatigue, but machines do not. Besides, it is unlikely that patients will undergo long-term manual real-time monitoring by doctors, but they could wear machines that have been validated for safety during a long time. Of course, safety is also a crucial issue that biomarkers and machine learning models need to face before being applied in clinical settings. We must conduct extensive theoretical verification and clinical trials to ensure the safety and reliability of these machine instructions.

Data availability

The code used in this article is provided in the **Supplementary Materials**.

Declaration of competing interest

The authors declare that they have no conflicts of interest in this work.

Acknowledgments

The authors have been funded with the Key Project of Beijing Municipal Commission of Science and Technology (Z221100007422016), the Joint Project of Beijing Natural Science Foundation (L222107), and the Sailing Project of Beijing Hospitals Authority in Clinical Medicine Development (ZLRK202319).

Supplementary materials

Supplementary material associated with this article can be found, in the online version, at doi:10.1016/j.fmre.2024.05.018.

References

[1] J.K. Krauss, N. Lipsman, T. Aziz, et al., Technology of deep brain stimulation: Current status and future directions, Nat. Rev. Neurol. 17 (2) (2021) 75–87.
[2] R.J. Piper, R.M. Richardson, G. Worrell, et al., Towards network-guided neuromodulation for epilepsy, Brain **145** (10) (2022) 3347–3362.
[3] M.J. Frank, J. Samanta, A.A. Moustafa, et al., Hold your horses: Impulsivity, deep brain stimulation, and medication in parkinsonism, Science 318 (5854) (2007) 1309–1312.
[4] S. Little, A. Pogosyan, S. Neal, et al., Adaptive deep brain stimulation in advanced Parkinson disease, Ann. Neurol. 74 (3) (2013) 449–457.

[5] K.W. Scangos, G.S. Makhoul, L.P. Sugrue, et al., State-dependent responses to intracranial brain stimulation in a patient with depression, Nat. Med. 27 (2) (2021) 229–231.
[6] K.W. Scangos, A.N. Khambhati, P.M. Daly, et al., Closed-loop neuromodulation in an individual with treatment-resistant depression, Nat. Med. 27 (10) (2021) 1696–1700.
[7] A.L. Benabid, S. Chabardes, J. Mitrofanis, et al., Deep brain stimulation of the subthalamic nucleus for the treatment of Parkinson's disease, Lancet Neurol. 8 (1) (2009) 67–81.
[8] A.A. Kühn, F. Kempf, C. Brücke, et al., High-frequency stimulation of the subthalamic nucleus suppresses oscillatory β activity in patients with Parkinson's disease in parallel with improvement in motor performance, J. Neurosci. 28 (24) (2008) 6165–6173.
[9] K.N. Fountas, J.R. Smith, A.M. Murro, et al., Implantation of a closed-loop stimulation in the management of medically refractory focal epilepsy: A technical note, Stereotact. Functional Neurosurg. 83 (4) (2005) 153–158.
[10] F.T. Sun, M.J Morrell, The RNS System: Responsive cortical stimulation for the treatment of refractory partial epilepsy, Exp. Rev. Med. Devices 11 (6) (2014) 563–572.
[11] V. Peterson, V. Kokkinos, E. Ferrante, et al., Deep net detection and onset prediction of electrographic seizure patterns in responsive neurostimulation, Epilepsia 64 (8) (2023) 2056–2069.
[12] M.G. Leguia, V.R. Rao, T.K. Tcheng, et al., Learning to generalize seizure forecasts, Epilepsia 64 (2023) S99–S113.
[13] S. Arcot Desai, M.F. Afzal, W. Barry, et al., Expert and deep learning model identification of iEEG seizures and seizure onset times, Front. Neurosci. 17 (2023) 1156838.
[14] S. Ghosh, J.K. Sinha, S. Ghosh, et al., A comprehensive review of emerging trends and innovative therapies in epilepsy management, Brain Sci. 13 (9) (2023) 1305.
[15] Y. Xia, M. Small, J. Wu, Introduction to focus issue: Complex network approaches to cyber-physical systems, Chaos 29 (9) (2019).
[16] S.J. Kiebel, J. Daunizeau, K.J Friston, A hierarchy of time-scales and the brain, PLoS Comput. Biol. 4 (11) (2008) e1000209.
[17] M.L. Kringelbach, A.R. McIntosh, P. Ritter, et al., The rediscovery of slowness: Exploring the timing of cognition, Trends Cog. Sci. 19 (10) (2015) 616–628.
[18] C. Meisel, K. Bailey, P. Achermann, et al., Decline of long-range temporal correlations in the human brain during sustained wakefulness, Sci. Rep. 7 (1) (2017) 11825.
[19] T. Montez, S.S. Poil, B.F. Jones, et al., Altered temporal correlations in parietal alpha and prefrontal theta oscillations in early-stage Alzheimer disease, Proc. Natl. Acad. Sci. 106 (5) (2009) 1614–1619.
[20] H. Jia, Y. Li, D. Yu, Attenuation of long-range temporal correlations of neuronal oscillations in young children with autism spectrum disorder, Neuroimage 20 (2018) 424–432.
[21] C.J. Markiewicz, K.J. Gorgolewski, F. Feingold, et al., The OpenNeuro resource for sharing of neuroscience data, Elife 10 (2021) e71774.
[22] G. Aiello, D. Ledergerber, T. Dubcek, et al., Functional network dynamics between the anterior thalamus and the cortex in deep brain stimulation for epilepsy, Brain 146 (11) (2023) 4717–4735.
[23] A. Schulze-Bonhage, M. Hirsch, S. Knake, et al., Focal cortex stimulation with a novel implantable device and antiseizure outcomes in 2 prospective multicenter single-arm trials, JAMA Neurol 80 (6) (2023) 588–596.
[24] J.M. Bernabei, A. Li, A.Y. Revell, et al., Quantitative approaches to guide epilepsy surgery from intracranial EEG, Brain 146 (6) (2023) 2248–2258.
[25] A. Delorme, S. Makeig, EEGLAB: An open source toolbox for analysis of single-trial EEG dynamics including independent component analysis, J. Neurosci. Methods 134 (1) (2004) 9–21.
[26] A.J. Myles, R.N. Feudale, Y. Liu, et al., An introduction to decision tree modeling, J. Chemometr. 18 (6) (2004) 275–285.
[27] F.J Yang, An implementation of naive bayes classifier, in: 2018 International Conference on Computational Science and Computational Intelligence (CSCI), IEEE, 2018, pp. 301–306.
[28] P.N. Belhumeur, J.P. Hespanha, D.J Kriegman, Eigenfaces vs. fisherfaces: Recognition using class specific linear projection, IEEE Trans. Pattern Anal. Mach. Intell. 19 (7) (1997) 711–720.
[29] J. Ahmad, C. Ellis, R. Leech, et al., From mechanisms to markers: Novel noninvasive EEG proxy markers of the neural excitation and inhibition system in humans, Transl. Psych. 12 (1) (2022) 467.
[30] V. Medel, M. Irani, N. Crossley, et al., Complexity and 1/f slope jointly reflect brain states, Sci. Rep. 13 (1) (2023) 21700.
[31] A. Pathania, M. Clark, R. Cowan, et al., Relating resting EEG power spectra to age-related differences in cognitive performance: An observational pilot study, MedRxiv (2021) 21251655.
[32] A.M. Van Nifterick, D. Mulder, D.J. Duineveld, et al., Resting-state oscillations reveal disturbed excitation–inhibition ratio in Alzheimer's disease patients, Sci. Rep. 13 (1) (2023) 7419.
[33] J.L. Molina, B. Voytek, M.L. Thomas, et al., Memantine effects on electroencephalographic measures of putative excitatory/inhibitory balance in schizophrenia, Biol. Psych. 5 (6) (2020) 562–568.
[34] V.O. Manyukhina, A.O. Prokofyev, I.A. Galuta, et al., Globally elevated excitation–inhibition ratio in children with autism spectrum disorder and below-average intelligence, Mol. Autism 13 (1) (2022) 20.
[35] A. Pathania, M. Schreiber, M.W. Miller, et al., Exploring the reliability and sensitivity of the EEG power spectrum as a biomarker, Int. J. Psychophysiol. 160 (2021) 18–27.
[36] T. Donoghue, M. Haller, E.J. Peterson, et al., Parameterizing neural power spectra into periodic and aperiodic components, Nat. Neurosci. 23 (12) (2020) 1655–1665.
[37] W. Huo, Z. Xia, Y. Gao, et al., Flexible thermoelectric devices with flexible heatsinks of phase-change materials and stretchable interconnectors of semi-liquid metals, ACS Appl. Mater. Interfaces 15 (24) (2023) 29330–29340.
[38] X. Huang, Y. Liu, G.W. Kong, et al., Epidermal radio frequency electronics for wireless power transfer, Microsyst. Nanoeng. 2 (1) (2016) 1–9.
[39] Y. LeCun, Y. Bengio, G. Hinton, Deep learning, Nature 521 (7553) (2015) 436–444.
[40] N. Khaleghi, S. Hashemi, S.Z. Ardabili, et al., Salient Arithmetic data extraction from brain activity via an improved deep network, Sensors 23 (23) (2023) 9351.
[41] G. Kozák, T. Földi, A. Berényi, Spike-and-wave discharges are not pathological sleep spindles, network-level aspects of age-dependent absence seizure development in rats, eNeuro 7 (1) (2020) ENEURO.0253-19.2019.
[42] V.R. Rao, J.D Rolston, Unearthing the mechanisms of responsive neurostimulation for epilepsy, Commun. Med. 3 (1) (2023) 166.
[43] M. Bange, G. Gonzalez-Escamilla, D.M. Herz, et al., Subthalamic stimulation modulates context-dependent effects of beta bursts during fine motor control, Nat. Commun. 15 (1) (2024) 3166.
[44] P. Kwan, M.J Brodie, Definition of refractory epilepsy: Defining the indefinable? Lancet Neurol. 9 (1) (2010) 27–29.

Author profile

Zhikai Yu received the B.S. degree from Shandong University, and now he is pursuing a PhD degree for neurosurgery. He is interested in explaining the principle of human brain with Neurological Computation methods mainly, but neurological modulation and biological electronics are also in his field.

Binghao Yang received the B.S. degree from Beijing Institute of Technology in 2019. He is currently pursuing the Ph.D. degree with the Institute of Automation, Chinese Academy of Sciences. His main research interests include neural dynamics and neural modulation with neuroelectrophysiological recording.

Jingjing Wang (BRID: 02099.00.60682) was graduated from School of Medicine, Tsinghua University in 2020. From 2015 to 2017, she conducted research as a visiting scholar at the University of Pittsburgh School of Medicine in the Neurological Lab, under the mentorship of professor Robert M. Friedlander, focusing on the mitochondrial damage mechanisms in neurodegenerative diseases. In 2020, she joined the Department of Neurosurgery at Xuanwu Hospital, Capital Medical University, and is currently a specialist trainee of neurosurgery. Her current research focuses on modeling and investigating the mechanisms of drug-resistant epilepsy.

Shan Yu is currently a professor with the Brainnetome Center and the National Laboratory of Pattern Recognition, the Institute of Automation, Chinese Academy of Sciences. He has authored or coauthored more than 30 peer-reviewed articles in neuroscience and other interdisciplinary fields at leading journals, such as the *Nature Machine Intelligence, the Journal of Neuroscience*, and *eLife*. His current research interests include neuronal information processing, brain-inspired computing, and brain–machine interface.